Reversibility of Pt-Skin and Pt-Skeleton Nanostructures in Acidic Media

ARTICLE *in* JOURNAL OF PHYSICAL CHEMISTRY LETTERS · FEBRUARY 2014

Impact Factor: 7.46 · DOI: 10.1021/jz4025707

THE JOURNAL OF PHYSICAL CHEMISTRY Letters

Letter

pubs.acs.org/JPCL

Reversibility of Pt-Skin and Pt-Skeleton Nanostructures in Acidic Media

Julien Durst,*[,†,∥] Miguel Lopez-Haro,[†,‡] Laetitia Dubau,[†] Marian Chatenet,[†,⊥] Yvonne Soldo-Olivier,[†] Laure Guétaz,[#] Pascale Bayle-Guillemaud,[‡] and Frédéric Maillard*[,†]

[†]Laboratoire d'Electrochimie et de Physico-chimie des Matériaux et des Interfaces, UMR 5279 CNRS/Grenoble-INP/Université de Savoie/Université Joseph Fourier, 1130 rue de la piscine, BP75, 38402 Saint Martin d'Hères Cedex, France

[‡]CEA, INAC/UJF-Grenoble 1, UMR-E, SP2M, LEMMA, Minatec, 38054 Grenoble Cedex 9, France

[#]CEA, LITEN, Département des Technologies de l'Hydrogène, Laboratoire des Composants PEM, 17 rue des Martyrs, 38054 Grenoble, France

[⊥]Member of the French University Institute (IUF)

Supporting Information

ABSTRACT: Following a well-defined series of acid and heat treatments on a benchmark Pt_3Co/C sample, three different nanostructures of interest for the electrocatalysis of the oxygen reduction reaction were tailored. These nanostructures could be sorted into the "Pt-skin" structure, made of one pure Pt overlayer, and the "Pt-skeleton" structure, made of 2−3 Pt overlayers surrounding the Pt−Co alloy core. Using a unique combination of high-resolution aberration-corrected STEM-EELS, XRD, EXAFS, and XANES measurements, we provide atomically resolved pictures of these different nanostructures, including measurement of the Pt-shell thickness forming in acidic media and the resulting changes of the bulk and core chemical composition. It is shown that the Pt-skin is reverted toward the Pt-skeleton upon contact with acid electrolyte. This change in structure causes strong variations of the chemical composition.

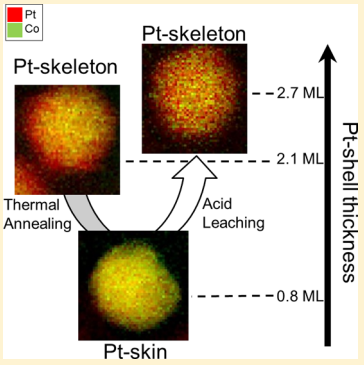

SECTION: Physical Processes in Nanomaterials and Nanostructures

The electrochemical activation of oxygen is the cornerstone of electrochemical energy conversion and storage devices, such as low-temperature proton-exchange fuel cells (PEMFCs), metal−air batteries, and electrolyzers. In acidic and oxidizing conditions, Pt is the only metal that can efficiently catalyze the oxygen reduction reaction (ORR), the reaction that limits the PEMFC performance.[1] One of the strategies to further improve the ORR kinetics is to alloy Pt with an early[2] or late[3−7] transition metal (referred to as M in what follows). The improved ORR activity of Pt−M electrocatalysts is attributed to a combination of strain and ligand effects. The strain effect causes a change in the electronic orbitals overlap, leading to a broadening of the d band of Pt, which results in a downshift of its average energy with respect to the Fermi level.[3,4,8−10] This in turn weakens the chemisorption energies of the ORR intermediates (OH, OOH, and O) and increases the rate of the ORR.[11] The ligand effect is due to the change in the electronic structure of the active sites by the neighboring M atoms[12−14] and causes similar variations of the chemisorption properties of Pt.

A major issue with bimetallic Pt−M electrocatalysts is the electrochemical dissolution of M atoms from the topmost surface layers in the oxidizing and acidic environment of a PEMFC cathode.[15−19] This electrochemical dissolution releases M^{z+} cations, which contaminate both the proton-exchange membrane (PEM) and the electrode ionomer, thereby depreciating their mass-transport properties.[20] To avoid this phenomenon, the mother Pt−M alloy is usually pretreated in an acidified solution[21] or dealloyed by cyclic voltammetry.[22,23] The dissolution of the non-noble 3d transition metal leaves behind an atomically rough surface composed of Pt atoms with low/no lateral coordination.[24,25] This nanostructure, first discovered by Toda et al.,[26,27] is currently referred to as a "Pt-skeleton" and maintains favorable catalytic properties toward the ORR if the Pt-shell is thin enough.[6,23,26,28−30] Another approach to form a pure Pt surface layer (one monolayer thick) is to thermally anneal the mother alloy, leading to the so-called "Pt-skin" nanostructure.[23,28] As stressed by Stamenkovic et al.[5,6] from measurements on single crystal surfaces and Wang et al.[25] on nanocrystallites, the thermal annealing restructures the near-surface region of the catalyst (it reduces the number of low coordination surface atoms), yielding the formation of (111) domains and compositional oscillations (the first and third monolayer (ML) become Pt-rich, while the second one enriches in M); overall, these effects

Received: November 26, 2013
Accepted: January 8, 2014

Table 1. Structural Parameters of the Pt_3Co/C-AT, the Pt_3Co/C-AT-HT, and the Pt_3Co/C-AT-HT-AT Samples Extracted from X-ray Diffractograms[a], TEM Images, X-EDS,[b] and X-ray Absorption Near Edge Structure (XANES) Spectra

	TEM	X-EDS	XRD		XNE
catalyst	$\bar{d}_N$ (nm)	at. comp.	$a_{(220)}$ (nm)	at. comp.	at. comp.
Pt_3Co/C-AT	3.9 ± 1.1	$Pt_{77\pm6}Co_{23\pm6}$	0.2706 ± 0.0003	$Pt_{75}Co_{25}$	$Pt_{70}Co_{30}$
Pt_3Co/C-AT-HT	4.0 ± 1.2	$Pt_{78\pm5}Co_{22\pm5}$	0.2725 ± 0.0003	$Pt_{82}Co_{18}$	$Pt_{73}Co_{27}$
Pt_3Co/C-AT-HT-AT	3.8 ± 1.0	$Pt_{86\pm7}Co_{14\pm7}$	0.2725 ± 0.0003	$Pt_{82}Co_{18}$	$Pt_{83}Co_{17}$

[a]The X-ray diffractogram errors are related to the instrumental resolution. In XRD, the Pt:Co atomic composition was determined using Vegard's law. [b]The X-EDS errors were determined from the standard deviation of at least 30 measurements.

contribute to the better ORR activity of the Pt-skin over the Pt-skeleton nanostructure and the mother alloy. Early studies performed by Chen et al.[28,31] have shown that the Pt-skin and Pt-skeleton nanostructures can be tailored at the nanometer scale, therefore opening a way to their use in real PEMFC devices. However, in such nanostructured materials, the beneficial effects of the alloying element depend primarily on the Pt-shell thickness and on the core chemical composition, that is the extent to which strain and ligand effects are operative.[29,32,33] Consequently, atomic imaging of the structural and chemical changes of these bimetallic Pt−M/C electrocatalysts in a model PEMFC environment is essential to know more about the economic viability of this model.

Due to the remarkable progress achieved over the past decade in transmission electron microscopy (TEM), such measurements are now possible on nanocrystallites. In particular, high-resolution aberration-corrected scanning transmission electron microscopy (HRSTEM) combined with electron energy-loss spectroscopy[22,34−40] in spectrum-imaging mode (EELS-SI) provides direct visualization of the elemental distribution in carbon-supported Pt−M nanoalloys. These two techniques were successfully used by Xin et al.[38] to evidence the facet-dependent surface segregation of Pt atoms in Pt_3Co/C nanocrystallites. Complementary to electron-based techniques, X-ray-based techniques probe the structure of bimetallic nanocatalysts with great statistical accuracy. In this paper, atomically resolved pictures of the different nanostructures that can be derived from a benchmark Pt_3Co/C catalyst in a model PEMFC environment were obtained. Using a unique combination of high-resolution aberration-corrected STEM-EELS, X-ray diffraction (XRD), X-ray absorption near edge structure (XANES), and extended X-ray absorption fine structure (EXAFS) measurements, the Pt-shell thickness and the chemical composition of several Pt-skeleton and Pt-skin nanostructures were also measured.

Three samples of Pt_3Co/C nanoparticles supported on carbon (metal weight fraction, 50 wt %) with a mean Pt to Co atomic ratio of 4 were examined (Table 1). A commercial Pt_3Co/C with an average Co atomic percentage of ~23 ± 6 atom % (as estimated from X-ray energy dispersive spectroscopy (X-EDS) analyses) was acid-treated for 12 h in a stirred 1 M H_2SO_4 solution at T = 333 K. This sample is referred to as the Pt_3Co/C-AT electrocatalyst. A fraction of this powder was then washed with ultrapure water and heat-treated at T = 673 K under vacuum for 4 h to obtain the Pt_3Co/C-AT-HT electrocatalyst. Finally, a fraction of the heat-treated powder was again acid-treated for 12 h in a stirred solution of 1 M H_2SO_4 at T = 333 K (denoted hereafter as Pt_3Co/C-AT-HT-AT) to probe possible rearrangement of the catalyst nanostructure. The particle size distributions of the three samples overimposed (see Figure SI-1 in the Supporting Information), confirming that coarsening of the bimetallic nanoparticles did not proceed during the thermal annealing step at T = 673 K, in agreement with the findings of ref 41.

Figure 1 shows a series of representative EELS elemental maps obtained for the Pt_3Co/C samples after a first acid

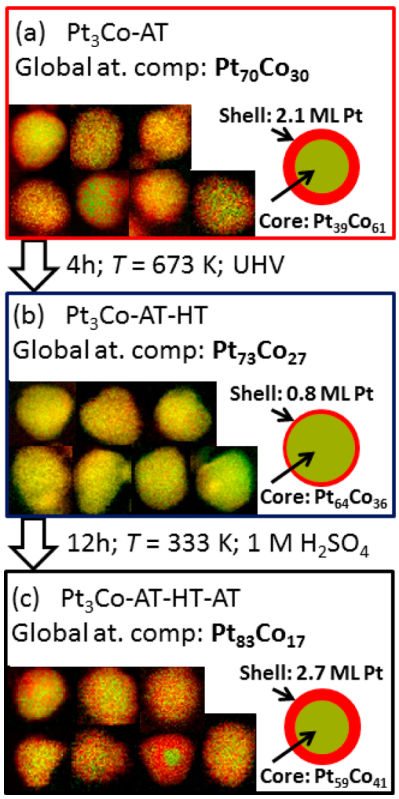

Figure 1. Structural and chemical modifications of Pt_3Co/C nanoparticles after several acid and thermal treatment steps. The elemental maps of (A) the Pt_3Co-AT, (B) the Pt_3Co-AT-HT, and (C) the Pt_3Co-AT-HT-AT individual nanoparticles were reconstructed from EELS-SI measurements performed at the Pt N_3 and at the Co $L_{2,3}$ edges. The Pt N_3 signal is shown in red, and the Co $L_{2,3}$ signal is shown in green. The global Pt/Co atomic composition (Global at. comp.) was determined from the XANES jump intensities recorded at the Pt L_{III} and at the Co K edges in transmission mode.

treatment (Figure 1a), after a subsequent thermal treatment (Figure 1b), and after a subsequent and final acid treatment (Figure 1c). The elemental distribution of Pt and Co atoms (color code: Pt in red and Co atoms in green) was reconstructed for individual nanoparticles by combining the EEL signal recorded at the Pt N_3 and at the Co $L_{2,3}$ edge using a power-law background subtraction (see Figures SI-2−SI-4 in the Supporting Information) for selected EEL spectra measured in the shell and in the core of the samples. Clearly, the final morphology of the catalysts depends on the latest treatment to

dx.doi.org/10.1021/jz4025707 | J. Phys. Chem. Lett. 2014, 5, 434−439

which they were subjected. In particular, the first acid treatment (Pt_3Co-AT) causes the formation of a Pt-skeleton structure with a 2.1 ± 0.5 ML thick Pt shell surrounding the mother Pt_3Co core (0.47 ± 0.18 nm; see Figure 2a). The error bar

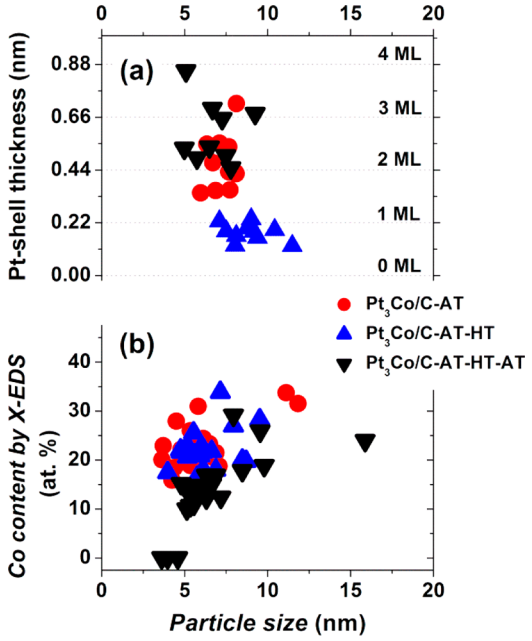

Figure 2. Atomic-scale morphology and chemical composition of the Pt_3Co/C-AT (red circles), the Pt_3Co/C-AT-HT (blue up-triangles), and the Pt_3Co/C-AT-HT-AT (black down-triangles) samples. (a) Histogram of the Pt-shell thickness and (b) chemical composition measured by X-EDS, represented as a function of the nanoparticle size.

represents the standard deviation over all measured shells. This result indicates that if any Co atoms were originally present at the surface and in the near-surface region of the nanoalloy, they were leached out during the acid treatment. Strikingly, the heat-treated Pt_3Co/C sample (Pt_3Co/C-AT-HT) hardly displays a segregated profile (Figure 1b). The statistical analysis performed on this sample indicates the presence of a 0.8 ± 0.3 ML thick Pt−shell on its surface, characteristic of Pt-skin structures (0.18 ± 0.06 nm; see Figure 2b). The heat treatment step has therefore promoted the diffusion of cobalt atoms to the subsurface region or, in other words, rehomogenized the distribution of Co atoms within the bulk of the nanoparticle. This result agrees with previous observations of Xin et al.[38] but is opposite to what was found by Wang et al.[25] These differences are believed to be due to the techniques used in both studies. Whereas Wang's conclusions are based on line-scan composition profiles obtained by energy-dispersive X-ray spectroscopy with an electron beam ∼2 Å in spot size scanning across individual catalyst particles, STEM-EELS was used to unveil the composition profiles at an atomic level in Xin's study[38] and in this work. Interestingly, the Pt-skin nanostructure is reverted to the Pt-skeleton upon exposure to the acidic and oxygen-containing electrolyte. Moreover, Figure 1c shows that during the second acid treatment, the Pt-shell thickens to 2.7 ± 0.6 ML (0.62 ± 0.24 nm) on the Pt_3Co-AT-HT-AT sample compared to the Pt-skin (Pt_3Co-AT-HT) and also compared to the first Pt-skeleton (Pt_3Co-AT) structures. The changes in nanostructure were not dependent on the particle size: core−shell nanoparticles were imaged whatever the size of the nanoparticles. However, measurements of the shell thickness were preferentially performed on nanocrystallites larger than 4−5 nm because of the instability of the smallest nanocrystallites under the high electron beam dose (Figure 2). Similar observations were recently made by Yu et al.[39]

Figure 3 shows the variations of the number of nearest Pt−Co neighbors extracted from the analysis of EXAFS spectra at

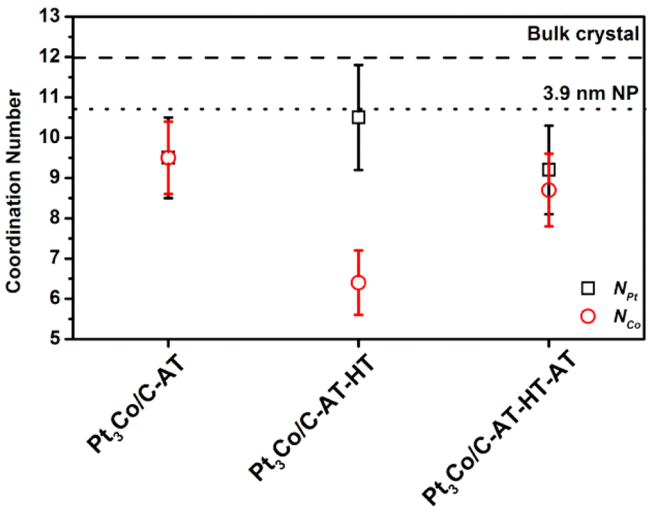

Figure 3. Total first-shell coordination numbers determined for Pt and Co environments (N_{Pt} in black open squares and N_{Co} in red open circles, respectively) for acid and vacuum-annealed Pt_3Co/C nanoparticles. The dashed line indicates the expected first-shell coordination number for a bulk face-centered cubic crystal, and the dotted line is for a 3.9 nm sized cuboctahedron.

the Pt L_{III} (N_{Pt}) and the Co K (N_{Co}) edges (see Figures SI-5 and SI-6 and Table SI-1 in the Supporting Information). Since the mean particle size remains constant for all samples, the changes of the first shell coordination numbers from one catalyst to another cannot be ascribed to size-induced variations of the mean coordination number but rather reflect different local ordering of Pt and Co atoms. For Pt_3Co/C-AT, the N values for platinum ($N_{Pt} = N_{Pt-Pt} + N_{Pt-Co}$) and cobalt atoms ($N_{Co} = N_{Co-Pt} + N_{Co-Co}$) are very close, N_{Pt} = 9.5 ± 1.0 versus N_{Co} = 9.5 ± 0.9. As expected from the nanometric dimensions of the Pt_3Co/C particles,[42] these values are smaller than the value of 12, which characterizes a bulk face-centered cubic structure. The results obtained for the Pt_3Co/C-AT-HT catalyst strongly differ; the average first-shell coordination is different whether the Pt or Co atomic environment is considered, N_{Pt} = 10.5 ± 1.3 and N_{Co} = 6.4 ± 0.8, in agreement with similar experimental trends reported on thermally annealed Pt_3Co/C[43,44] or PdCo/C nanoparticles.[45] In particular, a significant decrease of the Co−Co near the neighbors' numbers suggests the presence of Co atoms in the surface and near-surface layers (Table SI-1, Supporting Information); this model agrees with our EELS-SI observations. Finally, the data computed on the Pt_3Co/C-AT-HT-AT catalyst (N_{Pt} = 9.2 ± 1.1 versus N_{Co} = 8.7 ± 0.9) are similar to those obtained for the Pt_3Co/C-AT catalyst. Summing up, the EXAFS data suggest that the reversibility of the Pt-skin to the Pt-skeleton nanostructure also influences the local ordering of Pt and Co atoms.

We now focus on the changes of the chemical composition occurring during the acid and thermal treatments. For that purpose, XANES jump intensities at the Co K and the Pt L_{III}

dx.doi.org/10.1021/jz4025707 | J. Phys. Chem. Lett. 2014, 5, 434−439

edge (J_{Pt} and J_{Co}, respectively; see the Supporting Information for the detailed calculation) were measured in transmission mode, for which the absorption coefficient scales directly with the atomic composition. Such a methodology offers an advantage over X-EDS, also performed here for individual nanoparticles (see Figure 2b and Table 1) because it probes billions of nanoparticles (the electrodes used for the XAS analysis contained 5 mg_{Pt} cm^{-2}). Pt and Co atomic compositions (x_{Pt} and x_{Co}, respectively) were calculated as follows:

$$\frac{x_{Pt}}{x_{Co}} = \frac{J_{Pt}}{J_{Co}} \times 0.765$$

Similar chemical compositions were obtained for the Pt_3Co/C-AT and the Pt_3Co/C-AT-HT samples ($Pt_{70}Co_{30}$ versus $Pt_{73}Co_{27}$, respectively; see Table 1). This result was expected because the heat treatment only causes structural rearrangements but no removal/dissolution of either Pt or Co atoms. The XRD profiles obtained on these samples (Figure 4) clearly

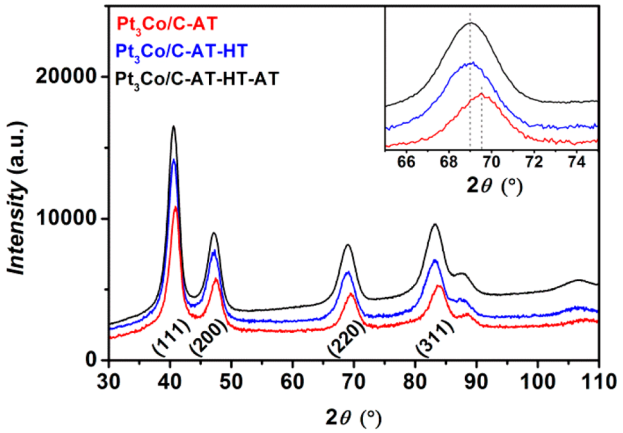

Figure 4. XRD patterns of the Pt_3Co/C-AT (red), the Pt_3Co/C-AT-HT (blue), and the Pt_3Co/C-AT-HT-AT (black) electrocatalysts. The inset is a zoom on the (220) diffraction peak used to determine interatomic distances of the samples.

reveal the shift of the X-ray reflections toward smaller 2θ values induced by the heat treatment; this signals a less strained lattice in the Pt-skin with respect to the Pt-skeleton structure, at the same nominal composition. Applying the classical Vegard's law to the acid-treated or heat-treated Pt−Co/C nanoparticles results in different chemical composition, $Pt_{75}Co_{25}$ and $Pt_{82}Co_{18}$ for the Pt_3Co/C-AT and Pt_3Co/C-AT-HT, respectively. This shows that local modifications of the surface and near-surface chemistry, such as those induced by acid or thermal treatment, cannot be detected by X-ray diffraction, which is mostly sensitive to the atomic composition of the bulk.

On Pt_3Co/C-AT-HT-AT, the overall Co content of the catalyst drops by more than 30% ($Pt_{83}Co_{17}$) upon exposure of the Pt-skin structure to an acidic environment: this confirms that Co atoms were removed from the second and third atomic layers of the Pt_3Co/C-AT-HT catalyst and agrees with the EELS-SI measurements (Figure 1). The atomic compositions calculated from XANES were confirmed from X-EDS analyses performed on individual nanoparticles for the three samples; a strong depletion in the average Co atom % is observed from the Pt_3Co/C-AT (23 ± 6 atom %) to the Pt_3Co/C-AT-HT-AT electrocatalyst (14 ± 7 atom %, Figure 2b). These results show that the structural reversibility does not translate into a chemical reversibility (Co atoms are lost during the second acid treatment). The depletion in Co depends on the nanocrystallite size, the smallest nanocrystallites being poorer in Co, in agreement with the experimental trends found by Chen et al.[28] In XRD, similar lattice parameters are extracted for the Pt_3Co/C-AT-HT and Pt_3Co/C-AT-HT-AT samples, which confirms that Vegard's law would have failed to provide the "true" chemical composition of the Pt_3Co/C-AT-HT and the Pt_3Co/C-AT-HT samples.

Finally, knowing the mean atomic Pt/Co composition and the detailed composition profiles (i.e. the Pt-shell thickness), the variations of the Pt/Co core composition were estimated (see Figure 1). Interestingly, the Pt/Co core compositions help rationalizing the variations of the lattice parameter determined by XRD. Indeed, the cobalt core content decreases from the Pt-skeleton to the Pt-skin but remains stable when reverting the Pt-skin to the Pt-skeleton and so do the XRD-derived Pt−Co compositions (Table 1). It is worth to say that such changes in nanostructure are of key importance for ORR electrocatalysis. Indeed, as explained earlier, the ability of the Pt overlayer to weaken the binding of O, OH, and OOH species and thus to improve the ORR activity is essentially related to the interplay of strain and ligand effects. Both effects are combined in the Pt-skin nanostructure, for which the second atomic layer is enriched in Co and the lattice is strained. The Pt-skin nanostructure however is not stable in a model PEMFC environment, where it is exposed to an open-circuit potential, acid, and an oxygen-containing electrolyte, and easily reverts to the Pt-skeleton nanostructure. The removal of Co atoms from the first 2−3 atomic layers greatly reduces the ligand effect on the topmost Pt surface overlayer and thus depreciates its ORR activity.[16,17,28]

In conclusion, we have provided atomically resolved pictures of different Pt_3Co nanostructures all derived from a commercially available Pt_3Co/C electrocatalyst into the Pt-skin nanostructure, made of one pure Pt overlayer, and the Pt-skeleton nanostructure, made of 2−3 Pt overlayers surrounding the mother core. We have outlined the reversibility of the Pt-skin nanostructure toward the Pt-skeleton nanostructure during acid treatment. This reversibility causes a large decrease of the overall Co content (by more than 30% in the present case) but no release of the lattice strain of the core material. These findings are of key importance for ORR electrocatalysis. The second major outcome of this study is that thermal annealing promotes the diffusion of bulk Co atoms toward the surface and near-surface layers, where they can be dissolved if the catalytic surface is exposed to an acidic environment. In that respect, the alternation of heat treatments (usually performed to homogenize the bulk composition in bimetallic alloys and smooth out surface defects and low coordination sites) and acid treatment should be avoided because it strongly decreases the core Co content and may cause contamination issues of the PEM/ionomer.[20] Finally, by comparing the information derived from XRD, EELS-SI, and XAS, we showed that local modifications of the surface and near-surface chemistry, such as those induced by acid or thermal treatment, cannot be detected by X-ray diffraction, which is mostly sensitive to the atomic composition of the core. An alternative method using the XANES jump intensities is proposed for a more accurate determination of the atomic composition of the nanoalloys.

dx.doi.org/10.1021/jz4025707 | J. Phys. Chem. Lett. 2014, 5, 434−439

■ ASSOCIATED CONTENT

Supporting Information

Further details of experimental methods, particle size distribution, EXAFS and EEL spectra, and details on the determination of the coordination number and atomic composition of the three samples based on the Pt L_{III} and Co K absorption spectra are provided. This material is available free of charge via the Internet at http://pubs.acs.org.

■ AUTHOR INFORMATION

Corresponding Authors

*E-mail: julien.durst@tum.de (J.D.).

*E-mail: frederic.maillard@lepmi.grenoble-inp.fr (F.M.).

Present Address

[‖]J.D.: Chair of Technical Electrochemistry, Technische Universität München, Lichtenbergstr. 4, D-85748 Garching, Germany.

Notes

The authors declare no competing financial interest.

■ ACKNOWLEDGMENTS

This work was funded by Oseo-Anvar in the framework of the H2E projects. The authors thank Dr. Jean-Louis Hazemann, Dr. Olivier Proux, and all of the members of the FAME team for their kind help to the realization of the EXAFS measurements on the beamline BM30B of the European Synchrotron Radiation Facility. The XAS measurements were performed in the frame of the Projects 30-02 1025 and 30-02 1054 "Surface reactivity and durability of Pt_3Co/C nanoparticles in proton-exchange membrane fuel cells". The help of Dr. Eric Sibert and Dr. Manuel Maréchal during the EXAFS measurements, and Dr. Stephane Coindeau for XRD measurements is also gratefully acknowledged. J.D. thanks Prof. Dr. Andrea E. Russell for the fruitful discussion regarding the EXAFS data in the frame of his Ph.D. thesis dissertation. M.C. thanks the French University Institute for its support.

■ REFERENCES

(1) Gasteiger, H. A.; Markovic, N. M. Just a Dream-or Future Reality? *Science* **2009**, *324*, 48−49.

(2) Stephens, I. E. L.; Bondarenko, A. S.; Gronbjerg, U.; Rossmeisl, J.; Chorkendorff, I. Understanding the Electrocatalysis of Oxygen Reduction on Platinum and Its Alloys. *Energy Environ. Sci.* **2012**, *5*, 6744−6762.

(3) Stamenkovic, V.; Mun, B. S.; Mayrhofer, K. J. J.; Ross, P. N.; Markovic, N. M.; Rossmeisl, J.; Greeley, J.; Norskov, J. K. Changing the Activity of Electrocatalysts for Oxygen Reduction by Tuning the Surface Electronic Structure. *Angew. Chem., Int. Ed.* **2006**, *45*, 2897−2901.

(4) Stamenkovic, V.; Schmidt, T. J.; Ross, P. N.; Markovic, N. M. Surface Composition Effects in Electrocatalysis: Kinetics of Oxygen Reduction on Well-Defined Pt_3Ni and Pt_3Co Alloy Surfaces. *J. Phys. Chem. B* **2002**, *106*, 11970−11979.

(5) Stamenkovic, V. R.; Mun, B. S.; Arenz, M.; Mayrhofer, K. J. J.; Lucas, C. A.; Wang, G. F.; Ross, P. N.; Markovic, N. M. Trends in Electrocatalysis on Extended and Nanoscale Pt-Bimetallic Alloy Surfaces. *Nat. Mater.* **2007**, *6*, 241−247.

(6) Stamenkovic, V. R.; Mun, B. S.; Mayrhofer, K. J. J.; Ross, P. N.; Markovic, N. M. Effect of Surface Composition on Electronic Structure, Stability, and Electrocatalytic Properties of Pt−Transition Metal Alloys: Pt-Skin versus Pt-Skeleton Surfaces. *J. Am. Chem. Soc.* **2006**, *128*, 8813−8819.

(7) Long, N. V.; Yang, Y.; Minh Thi, C.; Minh, N. V.; Cao, Y.; Nogami, M. The Development of Mixture, Alloy, and Core−Shell Nanocatalysts with Nanomaterial Supports for Energy Conversion in Low-Temperature Fuel Cells. *Nano Energy* **2013**, *2*, 636−676.

(8) Paffett, M. T.; Daube, K. A.; Gottesfeld, S.; Campbell, C. T. Electrochemical and Surface Science Investigations of PtCr Alloy Electrodes. *J. Electroanal. Chem.* **1987**, *220*, 269−285.

(9) Bardi, U.; Beard, B. C.; Ross, P. N. Surface Oxidation of a $Pt_{80}Co_{20}$ Alloy — An X-ray Photoelectron Spectroscopy and Low Energy Electron Diffraction Study on the [100] and [111] Oriented Single Crystal Surfaces. *J. Vac. Sci. Technol., A* **1988**, *6*, 665−670.

(10) Paffett, M. T.; Beery, J. G.; Gottesfeld, S. Oxygen Reduction at $Pt_{0.65}Cr_{0.35}$, $Pt_{0.2}Cr_{0.8}$ and Roughened Platinum. *J. Electrochem. Soc.* **1988**, *135*, 1431−1436.

(11) Hammer, B.; Norskov, J. K. Electronic Factors Determining the Reactivity of Metal Surfaces. *Surf. Sci.* **1995**, *343*, 211−220.

(12) Gauthier, Y.; Joly, Y.; Baudoing, R.; Rundgren, J. Surface-Sandwich Segregation on Nondilute Bimetallic Alloys: $Pt_{50}Ni_{50}$ and $Pt_{78}Ni_{22}$ Probed by Low-Energy Electron Diffraction. *Phys. Rev. B* **1985**, *31*, 6216−6218.

(13) Kitchin, J. R.; Norskov, J. K.; Barteau, M. A.; Chen, J. G. Role of Strain and Ligand Effects in the Modification of the Electronic and Chemical Properties of Bimetallic Surfaces. *Phys. Rev. Lett.* **2004**, *93*, 156801/1−156801/4.

(14) Bligaard, T.; Nørskov, J. K. Ligand Effects in Heterogeneous Catalysis and Electrochemistry. *Electrochim. Acta* **2007**, *52*, 5512−5516.

(15) Dubau, L.; Maillard, F.; Chatenet, M.; Guétaz, L.; André, J.; Rossinot, E. Durability of Pt_3Co/C Cathodes in a 16 Cell PEMFC Stack: Macro/Microstructural Changes and Degradation Mechanisms. *J. Electrochem. Soc.* **2010**, *157*, B1887−B1895.

(16) Dubau, L.; Maillard, F.; Chatenet, M.; André, J.; Rossinot, E. Nanoscale Compositional Changes and Modification of the Surface Reactivity of Pt_3Co/C Nanoparticles During Proton-Exchange Membrane Fuel Cell Operation. *Electrochim. Acta* **2010**, *56*, 776−783.

(17) Chen, S.; Gasteiger, H. A.; Hayakawa, K.; Tada, T.; Shao-Horn, Y. Platinum-Alloy Cathode Catalyst Degradation in Proton Exchange Membrane Fuel Cells: Nanometer-Scale Compositional and Morphological Changes. *J. Electrochem. Soc.* **2010**, *157*, A82−A97.

(18) Dubau, L.; Durst, J.; Maillard, F.; Guétaz, L.; Chatenet, M.; André, J.; Rossinot, E. Further Insights into the Durability of Pt_3Co/C Electrocatalysts: Formation of "Hollow" Pt Nanoparticles Induced by the Kirkendall Effect. *Electrochim. Acta* **2011**, *56*, 10658−10667.

(19) Dubau, L.; Lopez-Haro, M.; Castanheira, L.; Durst, J.; Chatenet, M.; Bayle-Guillemaud, P.; Guétaz, L.; Caqué, N.; Rossinot, E.; Maillard, F. Probing the Structural and Compositional Evolution of Pt_3Co/C Nanocrystallites during a 3422 h PEMFC Aging Test. *Appl. Catal., B* **2013**, *142*, 801−808.

(20) Durst, J.; Chatenet, M.; Maillard, F. Impact of Metal Cations on the Electrocatalytic Properties of Pt/C Nanoparticles at Multiple Phase Interfaces. *Phys. Chem. Chem. Phys.* **2012**, *14*, 13000−13009.

(21) Gasteiger, H. A.; Kocha, S. S.; Sompalli, B.; Wagner, F. T. Activity Benchmarks and Requirements for Pt, Pt-Alloy, and Non-Pt Oxygen Reduction Catalysts for PEMFCs. *Appl. Catal., B* **2005**, *56*, 9−35.

(22) Gan, L.; Heggen, M.; Rudi, S.; Strasser, P. Core−Shell Compositional Fine Structures of Dealloyed Pt_xNi_{1-x} Nanoparticles and Their Impact on Oxygen Reduction Catalysis. *Nano Lett.* **2012**, *12*, 5423−5430.

(23) Oezaslan, M.; Hasché, F.; Strasser, P. Pt-Based Core−Shell Catalyst Architectures for Oxygen Fuel Cell Electrodes. *J. Phys. Chem. Lett.* **2013**, *4*, 3273−3291.

(24) Wan, L. J.; Moriyama, T.; Ito, M.; Uchida, H.; Watanabe, M. *In Situ* STM Imaging of Surface Dissolution and Rearrangement of a Pt−Fe Alloy Electrocatalyst in Electrolyte Solution. *Chem. Commun.* **2002**, 58−59.

(25) Wang, C.; Chi, M.; Li, D.; Strmcnik, D.; van der Vliett, D.; Wang, G.; Komanicky, V.; Chang, K.-C.; Paulikas, A. P.; Tripkovic, D.; Pearson, J.; More, K. L.; Markovic, N. M.; Stamenkovic, V. R. Design and Synthesis of Bimetallic Electrocatalyst with Multilayered Pt-Skin Surfaces. *J. Am. Chem. Soc.* **2011**, *133*, 14396−14403.

(26) Toda, T.; Igarashi, H.; Uchida, H.; Watanabe, M. Enhancement of the Electroreduction of Oxygen on Pt Alloys with Fe, Ni, and Co. *J. Electrochem. Soc.* **1999**, *146*, 3750−3756.
(27) Toda, T.; Igarashi, H.; Watanabe, M. Role of Electronic Property of Pt and Pt Alloys on Electrocatalytic Reduction of Oxygen. *J. Electrochem. Soc.* **1998**, *145*, 4185−4188.
(28) Chen, S.; Sheng, W. C.; Yabuuchi, N.; Ferreira, P. J.; Allard, L. F.; Shao-Horn, Y. Origin of Oxygen Reduction Reaction Activity on "Pt_3Co" Nanoparticles: Atomically Resolved Chemical Compositions and Structures. *J. Phys. Chem. C* **2009**, *113*, 1109−1125.
(29) Strasser, P.; Koh, S.; Anniyev, T.; Greeley, J.; More, K.; Yu, C.; Liu, Z.; Kaya, S.; Nordlund, D.; Ogasawara, H.; Toney, M. F.; Nilsson, A. Lattice-Strain Control of the Activity in Dealloyed Core−Shell Fuel Cell Catalysts. *Nat. Chem.* **2010**, *2*, 454−460.
(30) Stephens, I. E. L.; Bondarenko, A. S.; Bech, L.; Chorkendorff, I. Oxygen Electroreduction Activity and X-ray Photoelectron Spectroscopy of Platinum and Early Transition Metal Alloys. *Chem. Catal. Chem* **2012**, *4*, 341−349.
(31) Chen, S.; Ferreira, P. J.; Sheng, W. C.; Yabuuchi, N.; Allard, L. F.; Shao-Horn, Y. Enhanced Activity for Oxygen Reduction Reaction on "Pt_3Co" Nanoparticles: Direct Evidence of Percolated and Sandwich-Segregation Structures. *J. Am. Chem. Soc.* **2008**, *130*, 13818−13819.
(32) Schlapka, A.; Lischka, M.; Groß, A.; Käsberger, U.; Jakob, P. Surface Strain Versus Substrate Interaction in Heteroepitaxial Metal Layers: Pt on Ru(0001). *Phys. Rev. Lett.* **2003**, *91*, 016101/1−016101/4.
(33) Lischka, M.; Mosch, C.; Groß, A. Tuning Catalytic Properties of Bimetallic Surfaces: Oxygen Adsorption on Pseudomorphic Pt/Ru Overlayers. *Electrochim. Acta* **2007**, *52*, 2219−2228.
(34) Sasaki, K.; Wang, J. X.; Naohara, H.; Marinkovic, N.; More, K.; Inada, H.; Adzic, R. R. Recent Advances in Platinum Monolayer Electrocatalysts for Oxygen Reduction Reaction: Scale-Up Synthesis, Structure and Activity of Pt Shells on Pd Cores. *Electrochim. Acta* **2010**, *55*, 2645−2652.
(35) Yu, Z. Q.; Zhang, J. L.; Liu, Z. Y.; Ziegelbauer, J. M.; Xin, H. L.; Dutta, I.; Muller, D. A.; Wagner, F. T. Comparison between Dealloyed $PtCo_3$ and $PtCu_3$ Cathode Catalysts for Proton Exchange Membrane Fuel Cells. *J. Phys. Chem. C* **2012**, *116*, 19877−19885.
(36) Oezaslan, M.; Heggen, M.; Strasser, P. Size-Dependent Morphology of Dealloyed Bimetallic Catalysts: Linking the Nano to the Macro Scale. *J. Am. Chem. Soc.* **2012**, *134*, 514−524.
(37) Dutta, I.; Carpenter, M. K.; Balogh, M. P.; Ziegelbauer, J. M.; Moylan, T. E.; Atwan, M. H.; Irish, N. P. Electrochemical and Structural Study of a Chemically Dealloyed PtCu Oxygen Reduction Catalyst. *J. Phys. Chem. C* **2010**, *114*, 16309−16320.
(38) Xin, H. L. L.; Mundy, J. A.; Liu, Z. Y.; Cabezas, R.; Hovden, R.; Kourkoutis, L. F.; Zhang, J. L.; Subramanian, N. P.; Makharia, R.; Wagner, F. T.; Muller, D. A. Atomic-Resolution Spectroscopic Imaging of Ensembles of Nanocatalyst Particles across the Life of a Fuel Cell. *Nano Lett.* **2012**, *12*, 490−497.
(39) Yu, Y. C.; Xin, H. L. L.; Hovden, R.; Wang, D. L.; Rus, E. D.; Mundy, J. A.; Muller, D. A.; Abruna, H. D. Three-Dimensional Tracking and Visualization of Hundreds of Pt−Co Fuel Cell Nanocatalysts during Electrochemical Aging. *Nano Lett.* **2012**, *12*, 4417−4423.
(40) Wang, D. L.; Xin, H. L. L.; Hovden, R.; Wang, H. S.; Yu, Y. C.; Muller, D. A.; DiSalvo, F. J.; Abruna, H. D. Structurally Ordered Intermetallic Platinum−Cobalt Core−Shell Nanoparticles with Enhanced Activity and Stability as Oxygen Reduction Electrocatalysts. *Nat. Mater.* **2013**, *12*, 81−87.
(41) Oezaslan, M.; Hasche, F.; Strasser, P. *In Situ* Observation of Bimetallic Alloy Nanoparticle Formation and Growth Using High-Temperature XRD. *Chem. Mater.* **2011**, *23*, 2159−2165.
(42) Witkowska, A.; Di Cicco, A.; Principi, E. Local Ordering of Nanostructured Pt Probed by Multiple-Scattering XAFS. *Phys. Rev. B* **2007**, *76*, 104110/1−104110/12.
(43) Lai, F. J.; Sarma, L. S.; Chou, H. L.; Liu, D. G.; Hsieh, C. A.; Lee, J. F.; Hwang, B. J. Architecture of Bimetallic Pt_xCo_{1-x} Electrocatalysts for Oxygen Reduction Reaction as Investigated by X-ray Absorption Spectroscopy. *J. Phys. Chem. C* **2009**, *113*, 12674−12681.
(44) Lai, F. J.; Su, W. N.; Sarma, L. S.; Liu, D. G.; Hsieh, C. A.; Lee, J. F.; Hwang, B. J. Chemical Dealloying Mechanism of Bimetallic Pt−Co Nanoparticles and Enhancement of Catalytic Activity toward Oxygen Reduction. *Chem.—Eur. J.* **2010**, *16*, 4602−4611.
(45) Kim, D. S.; Kim, J. H.; Jeong, I. K.; Choi, J. K.; Kim, Y. T. Phase Change of Bimetallic PdCo Electrocatalysts Caused by Different Heat-Treatment Temperatures: Effect on Oxygen Reduction Reaction Activity. *J. Catal.* **2012**, *290*, 65−78.